Appl. Phys. B (2017) 123:260
DOI 10.1007/s00340-017-6835-3

Applied Physics B
Lasers and Optics

4-nm continuous rapid sweeping spectroscopy in 2-μm band using distributed Bragg reflector laser

M. Abe[1,3] · T. Kanai[1,4] · N. Fujiwara[1,2] · Y. Ohiso[1] · H. Ishii[1] · M. Shimokozono[1] · H. Mastuzaki[1] · R. Kasahara[1] · M. Itoh[1]

Received: 25 January 2017 / Accepted: 21 September 2017 / Published online: 4 October 2017

Abstract We apply a newly developed 2-μm distributed Bragg reflector (DBR) laser to CO_2 spectroscopy. We achieve mode-hop free wavelength tuning over 4 nm by sweeping the DBR current and phase control current, simultaneously. The sensitivity of this laser spectroscopy system is better than 5×10^{-3}, which is the noise level, and means that a CO_2 concentration of 400 ppm can be detected with a path length of 1 m. We confirm that the DBR laser in the 2-μm region maintains a wide tunability of 4 nm even when rapidly swept at a scan rate of 10 kHz.

1 Introduction

Tunable diode lasers with a narrow linewidth are advantageous for gas spectroscopy because they make it possible to obtain fast and absolute measurements of species concentrations and flow parameters. In addition, these lasers are very attractive for practical applications owing to their compactness, reasonable cost, robustness and relative ease of use, and have been successfully applied to many gas species including NO, N_2O, CO, CO_2, O_2, CH_3Cl, CH_4, H_2O, and NH_3 in a variety of environments [1–4]. Telecom-qualified distributed feedback (DFB) lasers operating at 1.3–1.8 μm are especially useful because they provide low-noise and mode-hop free tuning characteristics, which are requirements for concentration measurements. Another advantage of these DFB-LDs is that light can be delivered through a fiber. They offer greater flexibility in terms of sensor design, which allows the realization of a remote gas sensor that operates under harsh environmental conditions.

The higher order overtones or combination bands of many gas species are probed using laser gas spectroscopy in this window. On the other hand, the absorbance of some molecules in the 2.0-μm region is much stronger than that in the 1.5-μm region. For example, the band strength of the CO_2 band near 2.01 μm is approximately a factor of 73 larger than the band near 1.58 μm [5]. As a result, laser absorption measurements near 2.0 μm improve the detection sensitivity of species concentration measurements without losing the benefit of fiber delivery.

The tunable wavelength range of DFB-LDs is limited to around a nanometer because wavelength tuning is achieved by a current-induced temperature change in the active region. The temperature response of the active layer also limits the current sweep speed of a DFB-LD to less than a few tens of kHz while maintaining the same wavelength tuning range [6]. On the other hand, distributed Bragg reflector (DBR) lasers enable wide and rapid wavelength tuning via current modulation. A DBR laser has an active region that provides optical gain and a DBR region whose refractive index can be changed by controlling the injection current. A wide wavelength tuning range of 5–10 nm is realized by controlling the injection current of the DBR region. DBR lasers operating in the 1.5-μm [7–10], 640-nm [11], 670-nm [12], 800-nm [13, 14], 860 and 990-nm [15] bands have already been developed and applied to laser sensing for various molecules [16, 17]. Recently, we successfully developed a

✉ M. Abe
abe@phys.chuo-u.ac.jp

1 NTT Device Technology Laboratories, NTT Corporation, Atsugi-Shi, Kanagawa 243-0198, Japan

2 NTT Device Innovation Center, NTT Corporation, Atsugi-Shi, Kanagawa 243-0198, Japan

3 Department of Physics, Faculty of Science and Technology, Chuo University, Bunkyo-ku, Tokyo 112-8551, Japan

4 NTT Access Network Service System Labs, NTT Corporation, Yokosuka-Shi, Kanagawa 239-0847, Japan

tunable DBR laser operating in the 2-μm region and reported continuous wavelength tuning of 5.6 nm along with a side mode suppression ratio (SMSR) of larger than 30 dB [18].

The aim of the present work is to extend the diode-laser sensor system to the sensitive measurement of CO_2 near 2.0 μm using a novel DBR laser. Spectroscopic measurements and sensors using many semiconductor lasers have already been developed [4, 19–23], but there has been no measurement using DBR in the 2 μm region. In this study, the injection current condition for continuous wavelength tuning of 4 nm is investigated, and the characteristics of a rapid scan at 10 kHz while maintaining a wide sweep range are described. We also measured CO_2 spectra from 2.012 to 2.016 μm (4959–4970 cm^{-1}) and compared the results with the HITRAN2012 database. The detection sensitivity of the sensor system is also determined.

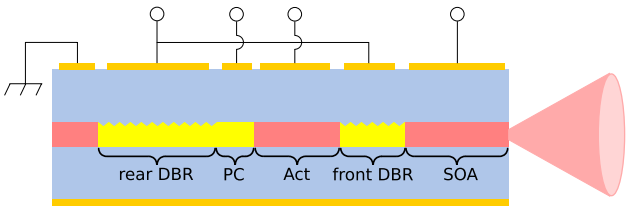

Fig. 1 Schematic diagram of 2-μm DBR laser cross-section. SOA: semiconductor optical amplifier region, front DBR: front DBR region, Act: active region, PC: phase control region, rear DBR: rear DBR region

2 2-μm DBR laser

Figure 1 shows a schematic drawing of the structure of our newly developed 2-μm DBR laser. This laser consists of a semiconductor optical amplifier (SOA) region, a front DBR region, an active region, a phase control (PC) region and a rear DBR region. Strained InGaAs multi-quantum wells (MQWs) are used in the active and SOA regions, and InGaAs is used for the passive layers of the DBR and PC region. The passive layers (the DBR and PC regions) were selectively regrown and butt-jointed to the active and SOA regions on an n-InP substrate. The design parameters are described in detail in Ref. [18].

To investigate the wavelength tuning characteristics of this laser diode, the DBR and phase sections were current-tuned in the 0 mA $\leq I_{DBR} \leq$ 20 mA and 0 mA $\leq I_{phase} \leq$ 20 mA ranges at $T = 25$ °C, where I_{DBR} and I_{phase} represent the currents injected into the DBR and the phase regions, respectively. Figure 2 shows a contour graph of the lasing emission wavelength monitored with an optical spectrum analyzer as a function of the DBR-section and phase-section currents. Here, the active section current I_{act} and the SOA section current I_{SOA} were fixed at 80 mA. The wavelength tuning range of the laser was found to be over 7 nm. The contours illustrated in Fig. 2 clearly show the boundaries at which discontinuities, i.e., mode hoppings occur. These repeated mode hoppings are observed approximately every 1 nm for the fabricated laser, so we understand

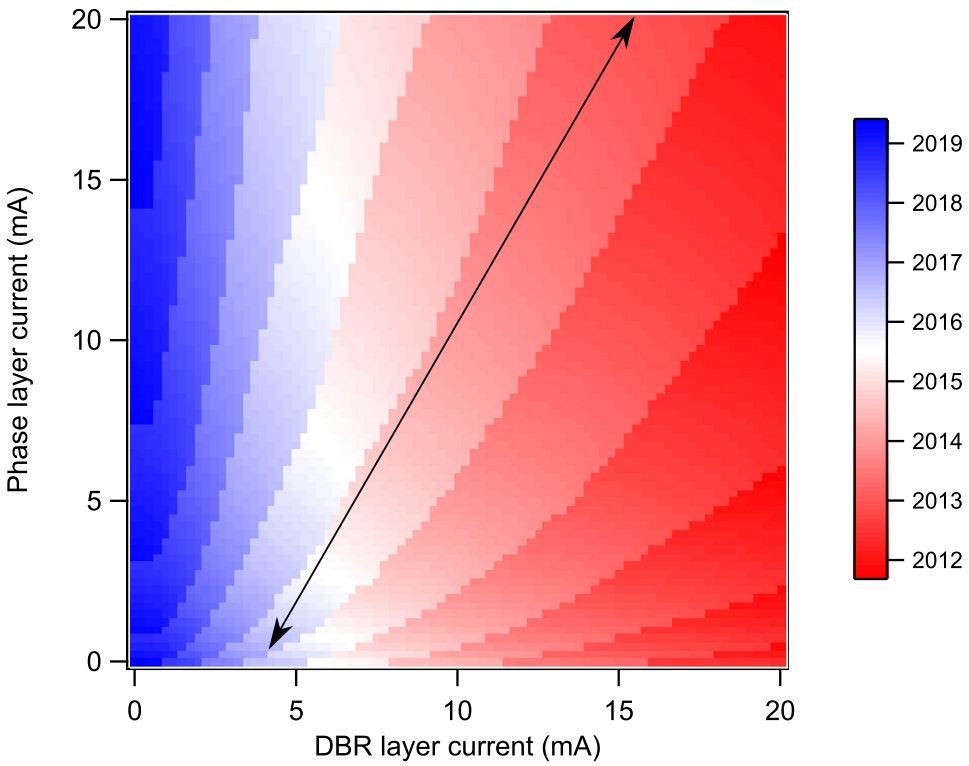

Fig. 2 Emission wavelength of the DBR laser as a function of the DBR and phase tuning currents, I_{DBR} and I_{phase}, with a fixed active layer current $I_{act} = 80$ mA and SOA layer current $I_{SOA} = 80$ mA. The right bar is in nanometer units. An arrow shows the condition where the DBR and PC currents are swept synchronously (Fig. 6b)

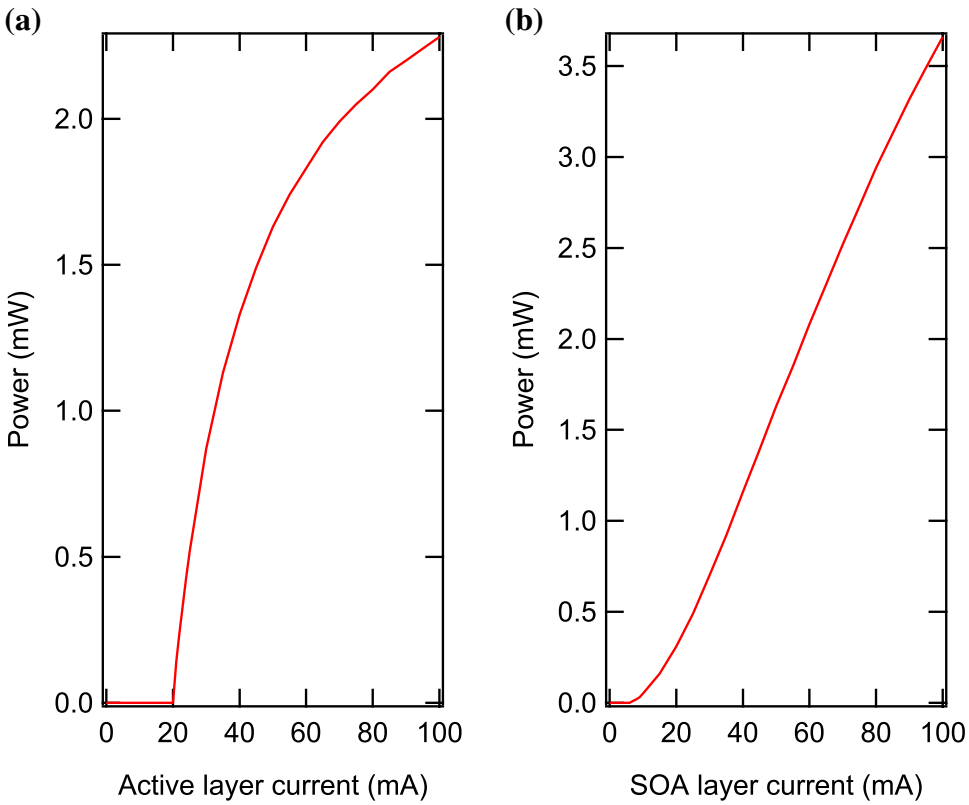

Fig. 3 Output power characteristic of the DBR laser as a function of the currents injected into the active and SOA layers. Here, I_{DBR} and I_{phase} are fixed at 0 mA. **a** shows the active layer current dependence when the SOA current was a constant 50 mA. **b** shows the SOA layer current dependence when the active current was a constant 50 mA

that a continuous molecular spectrum of, for example CO_2, N_2O, or NH_3, cannot be obtained when the DBR layer current or the phase layer current is tuned independently. On the other hand, we found that synchronous tuning of both the DBR layer and the phase layer currents enables continuous wavelength tuning without mode hopping. By repeating this DBR vs phase current tuning measurement, we observed a continuous wavelength tuning access condition of ~ 4 nm as mentioned in section IV.

Next, we checked the continuous wave (CW) operation characteristics of the DBR laser. Here, I_{DBR} and I_{phase} were fixed at 0 mA and the temperature was controlled at 25 °C. Figure 3a shows the active layer current dependence of the output power when the SOA layer current was fixed at 50 mA. We found that there was marked output power saturation for an active layer current of over 60 mA. By contrast, we observed the linear SOA current dependence of

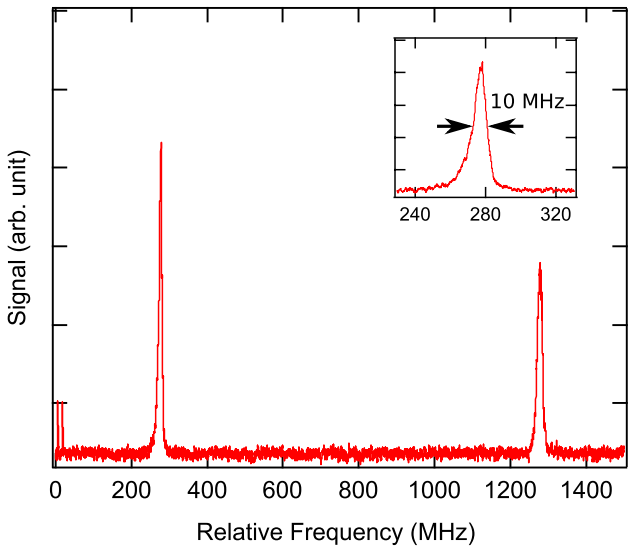

Fig. 4 Intensity versus frequency analysis of the DBR laser with a scanning Fabry–Perot etalon. The measurement was carried out with $I_{DBR} = 0$ mA, $I_{phase} = 0$ mA, $I_{act} = 80$ mA and $I_{SOA} = 80$ mA. The inset is the left resonance expanded. The observed resonance linewidth is 10 MHz

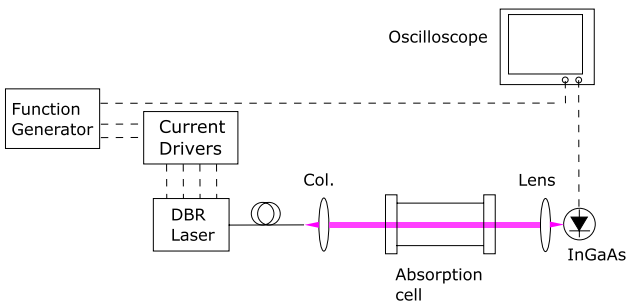

Fig. 5 Experimental setup. Col.: collimator lens, InGaAs: extended InGaAs detector. Dotted lines indicate electrical cables

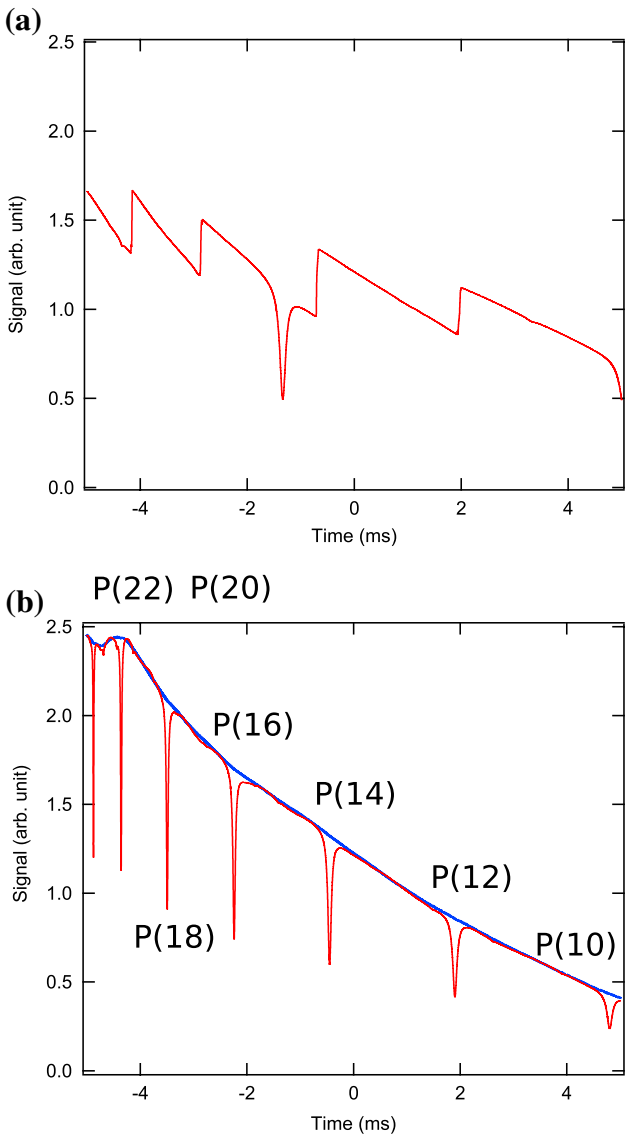

Fig. 6 Fine structure of the combination band $\nu_1 + 2\nu_2 + \nu_3$ of CO_2. **a** Spectrum when only changing the DBR current from 3.6 to 20.4 mA with 50 Hz up-sweep. The discontinuities correspond to the boundaries in Fig. 2. **b** Spectrum when sweeping the DBR and PC currents synchronously. The lasing wavelength was changed from 2012 to 2016 nm. The DBR current varied from 3.6 to 20.4 mA and the phase current varied from 0.3 to 29.0 mA. Seven strong lines were clearly obtained and these absorption lines correspond to P(22) to P(10). Eight scans of spectra were averaged. Additionally, a thick blue line shows the spectrum without the absorption cell

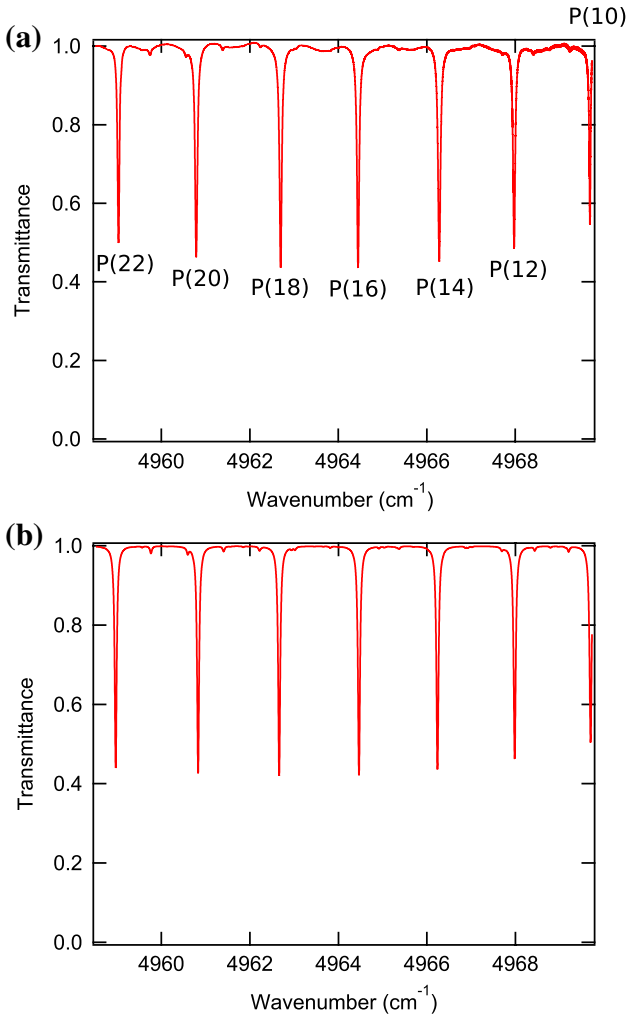

Fig. 7 Normalized (**a**) and calculated (**b**) spectra for CO_2 $\nu_1 + 2\nu_2 + \nu_3$ band: **a** is measured at room temperature; **b** is simulated using "SpectraPlot" under condition of partial pressures of 80 Torr for CO_2 and 110 Torr for air, and an absorption length of 20 cm at 300 K [24, 25]

the output power up to 100 mA when the active layer current was fixed at 50 mA (Fig. 3b). An output power of 3.7 mW was obtained with active and SOA layer currents of 100 mA.

The spectral linewidth of the DBR laser was measured using a piezo-electric transducer (PZT) scanning Fabry–Perot interferometer. The free spectral range (FSR) and finesse of the interferometer were 1 GHz and over 200, respectively. Figure 4 shows the transmitted intensity when the cavity was tuned over one FSR. The inset in Fig. 4 is an enlarged view of the left resonance line. The apparent linewidth (full-width at half-maximum, FWHM) was observed to be about 10 MHz when both the I_{DBR} and the I_{phase} were set at 0 mA. Note that the right resonance is small because one of mirrors of the Fabry–Perot etalon is misaligned at a position corresponding to the right resonance.

3 Experimental setup for CO_2 gas detection

Figure 5 shows the experimental setup for CO_2 gas detection using the DBR laser described in section II. A 2-μm output from the fiber was collimated with a collimating lens and injected in an absorption cell filled with CO_2 gas. The partial pressures of the CO_2 and air were 10.7 kPa (80 Torr) and

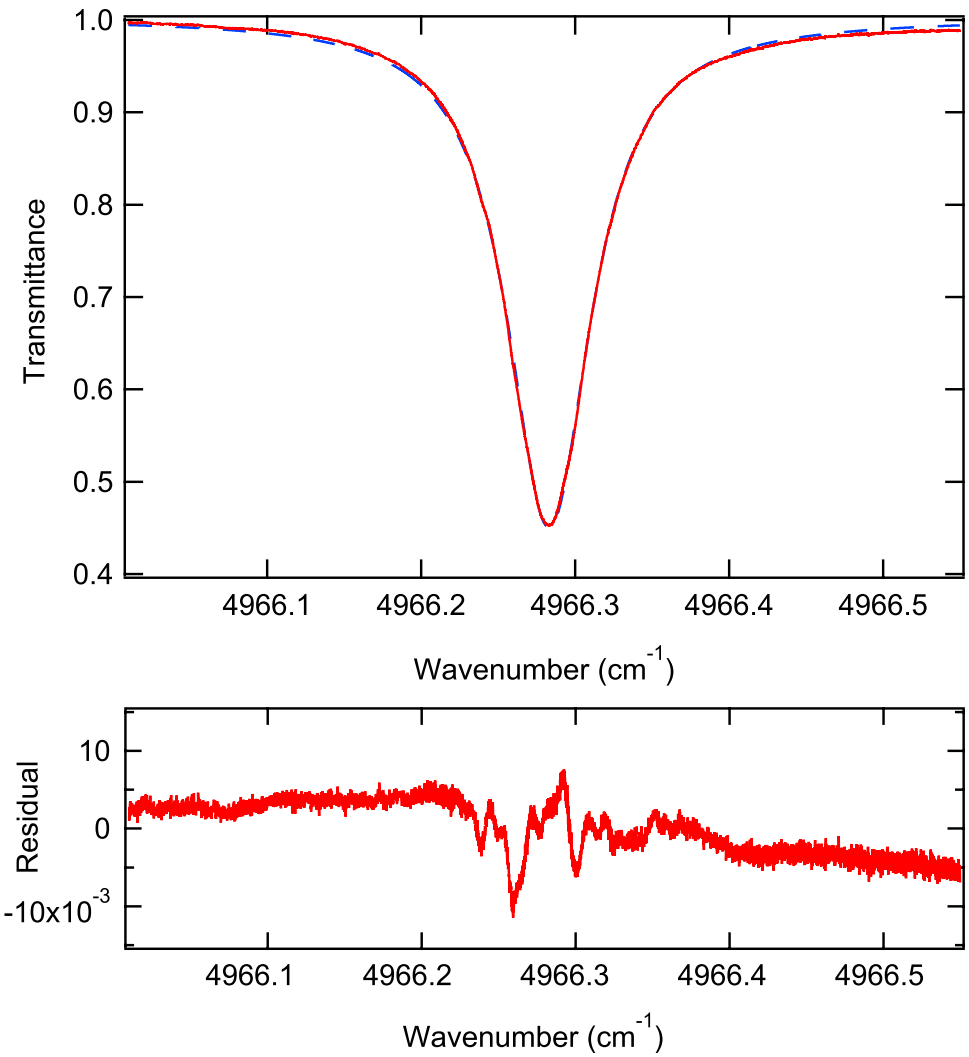

Fig. 8 Expanded spectrum of P(14) in Fig. 7. (Top) The red line is the measured data and the blue dots are a fitting curve. (Bottom) The difference between measured data and fitting

14.7 kPa (110 Torr), respectively. The cell was kept at room temperature. The output beam from the cell was focused with a lens that had a focal length of 100 mm and detected by an extended InGaAs detector. The detected signal was amplified with a trans-impedance amplifier and monitored by an oscilloscope with a 12-bit vertical resolution. The total bandwidth of the detection system was 100 MHz. The spectral absorbance was obtained by dividing the measured transmitted intensity by the reference intensity, which was obtained without the absorption cell.

Individual spectrum measurements were recorded by synchronously applying triangular waveforms to the injection currents of the DBR and phase layers via current drivers.

4 Results

Figure 6 shows the ro-vibrational spectrum of the combination band $\nu_1 + 2\nu_2 + \nu_3$ of CO_2 located at 2.01 μm measured with a scan speed of 50 Hz. The spectrum was averaged over eight times after filtering the signal from the detector with a low pass filter whose 3 dB cut-off was 80 kHz. Figure 6a shows the spectrum acquired simply by only changing the DBR current from 3.6 to 20.4 mA with up-sweep (the phase current is 0 mA). The observed discontinuities correspond with the mode hoppings, which are shown as boundaries in Fig. 2. On the other hand, a wide continuous wavelength scan was achieved from 2012 to 2016 nm without mode hopping by synchronously sweeping the DBR and PC currents (Fig. 6b). For this scan, the DBR current was varied from 3.6 to 20.4 mA and the PC current was varied from 0.3 to 29.0 mA as efficient current sweep was achieved. This corresponds to an arrow in Fig. 2. We clearly observed seven strong absorption lines, which are labeled P(22) to P(10). The wavelength separation between P(22) and P(10) is about 4 nm (12 cm^{-1}). The number inside the parentheses is the lower-state rotational angular momentum of carbon dioxide. The inequality of the absorption line separation in Fig. 6b is

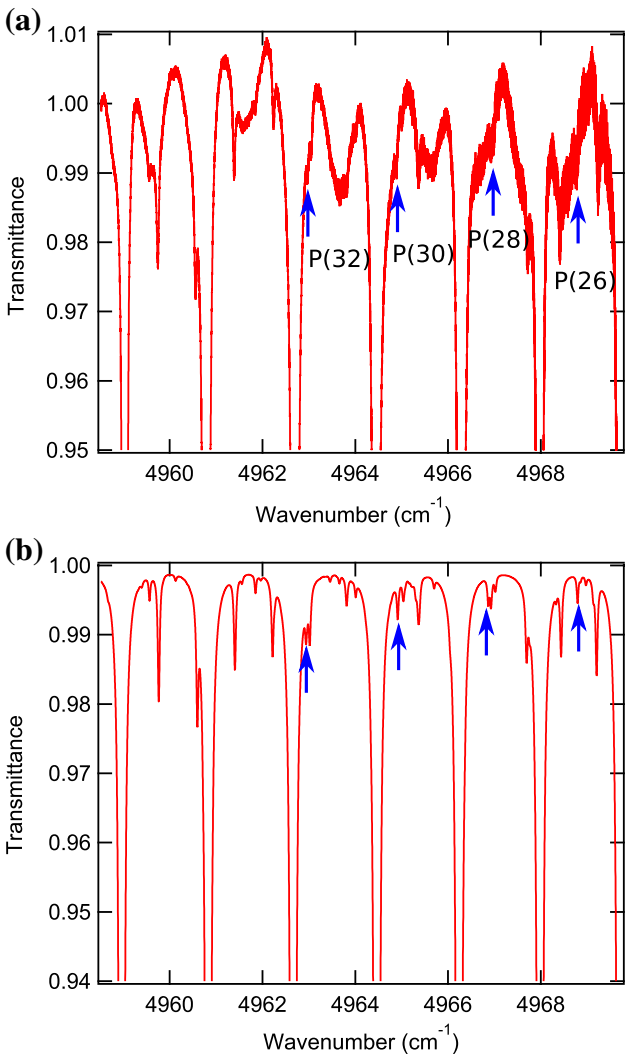

Fig. 9 Expanded spectra of Fig. 7. Normalized (**a**) and calculated (**b**) spectra. The arrows indicate $^{13}C^{16}O_2$ absorption lines

caused by the non-linear response of the wavelength tuning against currents applied to the DBR and the phase layers. Additionally, a thick blue line shows the spectrum without the absorption cell.

Figure 7a shows the normalized spectrum of CO_2. The spectrum was obtained by dividing the spectrum in Fig. 6b by the reference spectrum, which was acquired without the absorption cell. In this figure, the horizontal axis shows the lasing wavenumber. We calibrated the non-linearity between the wavenumber and the time relationship using the least square fitting method, whose coefficients we obtained from the observed CO_2 lines as markers. The fitting function is a 6th order polynomial and the line center uncertainty is 0.2 GHz. We carried out the fitting of observed seven absorption peaks using Lorentzian function. Figure 7b shows the calculated spectrum of CO_2 for 300 K based on HITRAN2012. The spectrum was calculated with using web-based simulating spectra

Table 1 Spectral data of the isotope CO_2 lines of the $\nu_1 + 2\nu_2 + \nu_3$ vibrational band, taken from the HITRAN2012 database [5]

Wavenumber (cm^{-1})	Intensity [cm^{-1}/(molecule/cm^{-2})]	Rotational state
$^{12}C^{16}O_2$		
4958.97	1.05×10^{-21}	P(22)
4960.83	1.13×10^{-21}	P(20)
4962.66	1.17×10^{-21}	P(18)
4964.47	1.19×10^{-21}	P(16)
4966.24	1.17×10^{-21}	P(14)
4967.98	1.11×10^{-21}	P(12)
4969.70	1.01×10^{-21}	P(10)
$^{13}C^{16}O_2$		
4958.90	2.08×10^{-24}	P(36)
4960.93	2.59×10^{-24}	P(34)
4962.93	3.16×10^{-24}	P(32)
4964.91	3.78×10^{-24}	P(30)
4966.87	4.43×10^{-24}	P(28)
4968.79	5.09×10^{-24}	P(26)

application "SpectraPlot" [24, 25]. The parameters we used for the calculation were the partial pressures of the CO_2 of 80 Torr and air of 110 Torr, respectively, and an absorption length of 20 cm. We found overall agreement between the experimentally obtained results and the calculated spectrum shape, although there was a slight difference. Figure 8 shows an expanded view of the measured and fitted spectra of P(14). The FWHM of each absorption line was found to be about 1.5 GHz (0.05 cm^{-1}), which was caused by pressure broadening and Doppler broadening. It is well known from Ref. [26] that the linewidth of a Voigt function is neither $\Delta\nu_D + \Delta\nu_h$ nor $(\Delta\nu_D^2 + \Delta\nu_h^2)^{1/2}$, when the Doppler width, $\Delta\nu_D$, and the homogeneous width, $\Delta\nu_h$, are present, where $\Delta\nu_h$ is considered to be pressure broadening. However, the linewidth of the Voigt function approaches $(\Delta\nu_D^2 + \Delta\nu_h^2)^{1/2}$ as $\Delta\nu_h/\Delta\nu_D$ increases. Under our experimental condition, calculation using the HITRAN database showed that the values of $2\Delta\nu_D$ and $2\Delta\nu_h$ are 0.28 and 1.55 GHz, respectively, and the Lorentzian function is verified for the fitting. We confirmed that the observed linewidth including uncertainty is consistent with the calculation.

The isotope absorption coefficient of $^{13}CO_2$ is two orders of magnitude weaker than that for the identical rotation–vibration transition of $^{12}CO_2$ because of its natural abundance. Figure 9 shows the expanded spectrum of the baseline. We observed many weak lines, which included the isotope $^{13}C^{16}O_2$ absorption lines. Table 1 shows the observable isotope CO_2 lines of the $\nu_1 + 2\nu_2 + \nu_3$ vibrational band referenced from the HITRAN2012 database [5]. Although six $^{13}C^{16}O_2$ lines are predicted to be located in this wavelength region, we observed only four lines, which are indicted with arrows, because two lines, P(34) and P(36), are overlapped by the strong $^{12}C^{16}O_2$

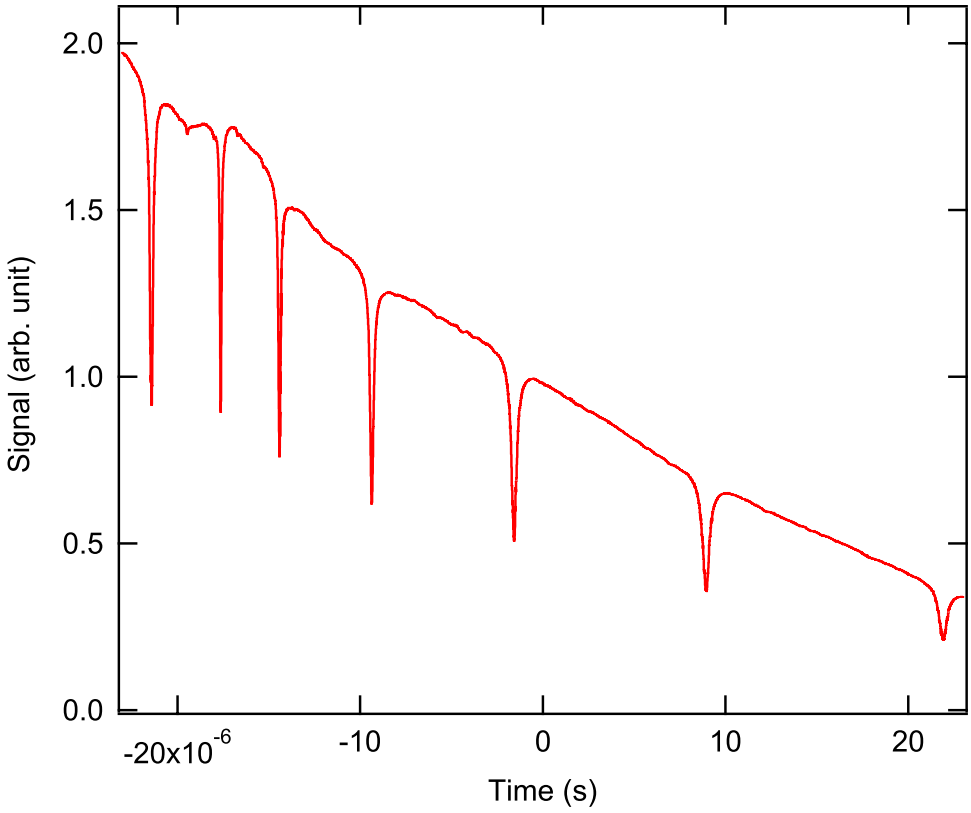

Fig. 10 Rapid current sweeping spectrum. This spectrum was acquired in only 50 μs and the scan wavelength range is 4 nm

lines. We observed the absorption line of P(32) of $^{13}C^{16}O_2$ whose intensity is three orders of magnitude weaker than that of $^{12}C^{16}O_2$ lines. We estimate that the noise level is less than 5×10^{-3}. On the other hand, the baseline has its own fluctuation of 1.4×10^{-2}. If we assume that the sensitivity of the optical sensing system is determined by the noise level, this noise level corresponds to the detection capability of the P(16) line of $^{12}C^{16}O_2$ in air whose concentration is 400 ppm with a pass length of 1 m. This is because a 1 m absorption of P(16) of $^{12}C^{16}O_2$ is calculated as 0.6% (6×10^{-3}) using approximate Eq. (1).

$$I(\nu) = I_0 \exp\left[-\frac{c}{k_B T}\frac{1}{\pi}\frac{\Delta\nu}{(\nu-\nu_0)^2+(\Delta\nu)^2} S p_{CO_2} l\right] \quad (1)$$

where I_0 is the incident intensity, c is the speed of light, k_B is the Boltzmann constant, T is temperature, S is the line intensity in HITRAN, p_{co_2} is the partial pressure of CO_2, ν_0 is the resonant frequency of the absorption, $\Delta\nu$ is the linewidth of the line, which is the air broadening coefficient ($\Delta\nu = 2.1$ GHz) (half width at half maximum, HWHM), and l is the absorption length [27].

Finally, we estimate the rapid sweep property of the DBR laser while maintaining a wide wavelength range. Figure 10 shows the spectrum when the DBR and phase currents are synchronously changed with 10 kHz triangle-waveform current modulation. A wide-band spectrum of 4 nm, whose bandwidth is the same as in Fig. 6b, was acquired in only 50 μs. We further investigated the rapid sweep property up to 40 kHz and verified that there is a mode hopping-free scanning range up to 3 nm. Over 50 kHz, we recognized mode hopping. We consider the reason is that the boundary in Fig. 2 changes and the arrow crosses over the boundary accordingly in the lower current region.

5 Conclusion

In summary, we reported the 2-μm wide and fast swept spectroscopy of CO_2 using a DBR laser. We demonstrated CO_2 gas detection using the developed spectrometer and investigated its detection sensitivity. The DBR laser possesses both a wide tunability, ~ 4 nm, and a rapid sweep speed, of over 10 kHz. CO_2 spectra between 2.012 and 2.016 μm (4959–4970 cm^{-1}) were measured and compared with the HITRAN2012 database. The DBR laser offers a rapid and wide-range sweep and an estimated detection sensitivity of $< 5 \times 10^{-3}$. With this DBR laser, it is possible to observe a plurality of absorption lines at a sweep rate of about 10 kHz while maintaining a wide tuning range, so that the concentration and temperature distribution in a high-speed transient phenomenon can be

detected. The applications of this 2-μm DBR laser range from spectroscopy in basic research to the industrial analysis of combustion.

Acknowledgements We are grateful to Dr. Y. Nishida of the NTT Electronics Corporation for invaluable support.

References

1. D.S. Baer, R.K. Hanson, M.E. Newfield, N.K.J.M. Gopaul, Opt. Lett. **19**, 1900 (1994)
2. S.-I. Chou, D.S. Baer, R.K. Hanson, Appl. Opt. **36**, 3288 (1997)
3. D.M. Sonnenfroh, M.G. Allen, Appl. Opt. **36**, 7970 (1997)
4. R. Mihalcea, M. Webber, D. Baer, R. Hanson, G. Feller, W. Chapman, Appl. Phys. B **67**, 283 (1998)
5. L. Rothman, I. Gordon, Y. Babikov, A. Barbe, D.C. Benner, P. Bernath, M. Birk, L. Bizzocchi, V. Boudon, L. Brown, A. Campargue, K. Chance, E. Cohen, L. Coudert, V. Devi, B. Drouin, A. Fayt, J.-M. Flaud, R. Gamache, J. Harrison, J.-M. Hartmann, C. Hill, J. Hodges, D. Jacquemart, A. Jolly, J. Lamouroux, R.L. Roy, G. Li, D. Long, O. Lyulin, C. Mackie, S. Massie, S. Mikhailenko, H. Muller, O. Naumenko, A. Nikitin, J. Orphal, V. Perevalov, A. Perrin, E. Polovtseva, C. Richard, M. Smith, E. Starikova, K. Sung, S. Tashkun, J. Tennyson, G. Toon, V. Tyuterev, G. Wagner, J. Quant. Spectrosc. Radiat. Transfer **130**, 4 (2013)
6. M. Fukuda, T. Mishima, N. Nakayama, T. Masuda, Appl. Phys. B **100**, 377 (2010)
7. M. Oishi, M. Yamamoto, K. Kasaya, IEEE Photon. Technol. Lett. **9**, 431 (1997)
8. M. Mitsuhara, M. Ogasawara, M. Oishi, H. Sugiura, K. Kasaya, IEEE Photon. Technol. Lett. **11**, 33 (1999)
9. T. Sato, M. Mitsuhara, T. Watanabe, K. Kasaya, T. Takeshita, Y. Kondo, IEEE J. Select. Topics Quantum Electron. **13**, 1079 (2007)
10. N. Fujiwara, T. Kakitsuka, M. Ishikawa, F. Kano, H. Okamoto, Y. Kawaguchi, Y. Kondo, Y. Yoshikuni, Y. Tohmori, IEEE J. Select. Topics Quantum Electron. **9**, 1132 (2003)
11. D. Feise, W. John, F. Bugge, C. Fiebig, G. Blume, K. Paschke, Opt. Express **20**, 23374 (2012)
12. M. Maiwald, J. Fricke, A. Ginolas, J. Pohl, B. Sumpf, G. Erbert, G. Trankle, Laser Photonic Rev. **7**, L30 (2013)
13. M. Uemukai, T. Suhara, Jpn. J. Appl. Phys. **55**, 08 (2016)
14. B. Sumpf, J. Kabitzke, J. Fricke, P. Ressel, A. Müller, M. Maiwald, G. Tränkle, Opt. Lett. **41**, 3694 (2016)
15. J.W. Zimmerman, R.K. Price, U. Reddy, N.L. Dias, J.J. Coleman, IEEE J. Select. Topics Quantum Electron. **19**, 1503712 (2013)
16. K. Boylan, V. Weldon, D. McDonald, J. O'Gorman, J. Hegarty, IEE Proc. Optoelectron. **148**, 19 (2001)
17. A.S. Diba, F. Xie, B. Gross, L.C. Hughes, C.-en Zah, F. Moshary. Opt. Express **23**, 27123 (2015)
18. T. Kanai, N. Fujiwara, Y. Ohiso, H. Ishii, M. Shimokozono, M. Itoh, IEICE Electron. Express **13**, 20160655 (2016)
19. P. Werle, F. Slemr, K. Maurer, R. Kormann, R. Mucke, B. Janker, Opt. Lasers Eng. **37**, 101 (2002)
20. M.E. Webber, S. Kim, S.T. Sanders, D.S. Baer, R.K. Hanson, Y. Ikeda, Appl. Opt. **40**, 821 (2001)
21. M.E. Webber, R. Claps, F.V. Englich, F.K. Tittel, J.B. Jeffries, R.K. Hanson, Appl. Opt. **40**, 4395 (2001)
22. R. Sur, K. Sun, J.B. Jeffries, R.K. Hanson, Appl. Phys. B **115**, 9–24 (2014)
23. G.B. Rieker, J.B. Jeffries, R.K. Hanson, Appl. Phys. B **94**, 51–63 (2009)
24. M. Spearrin, C. Goldenstein, C. Strand, V. Miller, SpectraPlot.com. http://www.spectraplot.com/
25. C.S. Goldenstein, V.A. Miller, R. Mitchell Spearrin, C.L. Strand, J. Quant. Spectrosc. Radiat. Transfer **200**, 249 (2017)
26. K. Shimoda, in High-Resolution Laser Spectroscopy, Topics in Applied Physics, K. Shimoda, ed. (Springer-Verlag, 1976), p. 23-25
27. M. Šimečková, D. Jacquemart, L.S. Rothman, R.R. Gamache, A. Goldman, J. Quant. Spectrosc. Radiat. Transfer **98**, 130 (2006)